Suppressed electric quadrupole collectivity in ^{32}Si

J. Heery,[1,*] J. Henderson,[1,†] C. R. Hoffman,[2,‡] A. M. Hill,[3,4] T. Beck,[4] C. Cousins,[1] P. Farris,[3,4] A. Gade,[3,4] S. A. Gillespie,[4] J. D. Holt,[5,6] B. Hu,[5] H. Iwasaki,[3,4] S. Kisyov,[7,§] A. N. Kuchera,[8] B. Longfellow,[7] C. Müller-Gatermann,[2] A. Poves,[9] E. Rubino,[4,∥] R. Russell,[1] R. Salinas,[3,4] A. Sanchez,[3,4] D. Weisshaar,[4] C. Y. Wu,[7] and J. Wu[4,¶]

[1]*School of Maths and Physics, University of Surrey, Guildford GU2 7XH, United Kingdom*
[2]*Physics Division, Argonne National Laboratory, Lemont, Illinois 60439, USA*
[3]*Department of Physics and Astronomy, Michigan State University, East Lansing, Michigan 48824, USA*
[4]*Facility for Rare Isotope Beams, Michigan State University, East Lansing, Michigan 48824, USA*
[5]*TRIUMF, Vancouver, British Columbia V6T 2A3, Canada*
[6]*Department of Physics, McGill University, Montréal, Québec H3A 2T8, Canada*
[7]*Lawrence Livermore National Laboratory, Livermore, California 94550, USA*
[8]*Department of Physics, Davidson College, Davidson, North Carolina 28035, USA*
[9]*Departamento de Fisica Teorica and IFT UAM-CSIC, Universidad Autonoma de Madrid, E-28049 Madrid, Spain*

(Received 8 August 2023; accepted 22 December 2023; published 25 January 2024)

Lying between ^{16}O and ^{40}Ca, the *sd* shell is well described by robust phenomenological and *ab initio* nuclear theories. In this work, however, we highlight an unexplained reduction in electric-quadrupole strength in the rare isotope ^{32}Si, studied through sub-barrier Coulomb excitation. It is found that the oblate nature of the deformation is well reproduced, while the absolute scale of quadrupole deformation, however, is inhibited by approximately a factor of 2 compared to theoretical predictions. Through comparison with shell-model and *ab initio* calculations, we present a number of possible explanations for this inhibited $E2$ strength. By comparing the results of these calculations to multiple observables, we conclude that there is a reduced role for out-of-space excitations in ^{32}Si, resulting in a reduction in the corrections normally applied to both models.

DOI: 10.1103/PhysRevC.109.014327

I. INTRODUCTION

Nuclear deformation is an emergent phenomenon, found across the nuclear landscape and manifesting most commonly in its quadrupole form. Its presence can be deduced from a number of features arising from the collective behavior of nucleons, such as low-lying quadrupole excitations (e.g., 2^+ states in even-even nuclei), enhanced electric quadrupole transition strengths [$B(E2)$ values], and large quadrupole moments (Q_s values). The degree to which quadrupole deformation dominates the low-lying structures of a nucleus is known to be closely related to the microscopic structure of the nucleus. For example, in the vicinity of magic numbers, a spherical stabilization occurs and deformation is strongly inhibited. Conversely, in mid-shell regions of the nuclear landscape, quadrupole deformation often dominates low-lying states, giving rise to structures akin to axial rotors.

The *sd* shell is an exceptional laboratory for nuclear physics, with a relatively modest valence space permitting full configuration-interaction calculations with no requirement for truncation. Alongside this, the region is home to almost the full range of nuclear structure phenomena, with examples of shell evolution, deformation, superdeformation, shape coexistence, single-particle structures, and the accessibility of the line of $N = Z$ [1–7]. Consequently, there exist incredibly robust nuclear models for the mass region, with well-understood scopes, and making use of both phenomenological and *ab initio* interactions [8–10].

In this article we present an intriguing conflict with these models, arising from a significantly inhibited degree of quadrupole collectivity in ^{32}Si, a nucleus for which the "gold standard" USD-based interactions are expected to perform well [11]. By performing a low-energy Coulomb excitation measurement of ^{32}Si we are able to conclusively resolve a prior experimental discrepancy in $B(E2; 0_1^+ \to 2_1^+)$ values [12–14], infer the form of the quadrupole deformation in ^{32}Si, and further confer some additional validation upon the only existing measurement of $B(E2; 0_1^+ \to 2_1^+)$ in ^{34}Si [14].

*j.heery@surrey.ac.uk
†jack.henderson@surrey.ac.uk
‡crhoffman@anl.gov
§Present address: Accelerator Technology and Applied Physics Division, Lawrence Berkeley National Laboratory, Berkeley, California 94720, USA.
∥Present address: Lawrence Livermore National Laboratory, Livermore, California 94550, USA.
¶Present address: National Nuclear Data Center, Brookhaven National Laboratory, Upton, New York 11973, USA.

II. EXPERIMENT AND ANALYSIS

The experiment was performed at the Re-accelerator facility (ReA6) [15] of the National Superconducting Cyclotron Laboratory (NSCL) [16]. A sample of ^{32}Si ($T_{1/2} = 153(7)$ years [17]) was acquired from Oak Ridge National Laboratory. It was then ionized in the batch mode ion source from where it was injected into the ReA6 accelerator chain. Contaminants of ^{96}Mo and ^{32}S were identified in the beam after acceleration. The experiment can be separated into two running modes. In the first ("contaminated"), the beam was delivered to the experimental station at a total rate of $\approx 5 \times 10^5$ pps, without any intervention to suppress the ^{96}Mo. In the second ("uncontaminated") a foil was used to strip the accelerated cocktail beam, suppressing the ^{96}Mo entirely. Note that the ^{32}S contaminant was present in both configurations, albeit at different levels, and was monitored intermittently to be treated in the Coulomb-excitation analysis. As a consequence of energy loss in the stripper foil, the on-target energies were 3.57 and 3.48 MeV/u for the contaminated and uncontaminated modes, respectively.

The accelerated beam was then impinged upon a 1.59 mg/cm^2 ^{196}Pt target, located in the JANUS setup [18]. The target contained a small amount of ^{194}Pt ($\approx$2.5%), which has been accounted for in the analysis. JANUS consists of a pair of S3-type [19] annular double-sided silicon detectors located upstream and downstream of the target. The downstream S3 detector covers an angular range in the center-of-mass frame of 25°–136°. For these angles, the minimum impact parameters are $\geqslant$5.4 fm for both the higher and lower beam energies, which satisfies Cline's 5 fm safe-distance criterion for low-energy Coulomb excitation [20], thus suppressing excitation due to the strong nuclear force. The upstream S3 detector covers an angular range in the center-of-mass frame of 140°–164°. For these angles, the minimum impact parameters are 4.8–5.3 and 5.3–5.7 fm for the higher and lower beam energies, respectively. Since 4.8 fm is below Cline's safe-distance criterion, the subset of data taken in the upstream S3 detector for the higher beam energy were excluded from the analysis; however, we note that including these angles in the analysis did not greatly impact the final results. The S3 detectors were surrounded by the Segmented Germanium Array (SeGA) [21], which comprises 16 detectors mounted in a barrel configuration, for γ-ray detection. Data were acquired through a digital system made up of 100 MHz (SeGA) and 250 MHz (silicon) XIA Pixie-16 modules, running in a triggerless continuous-running mode. The data were analyzed using the GRUTINIZER [22] software package, built in a ROOT framework [23].

^{32}Si events were constructed from coincident signals in the rings and segments of the downstream and upstream S3 detectors based on temporal and energetic conditions. γ rays detected in SeGA were corrected for their Doppler shift on the basis of the reaction kinematics and the respective angles of the recoiling nucleus and γ-ray detection. Beam (^{32}Si) and target (^{196}Pt) events could be distinguished by their energy deposition in the S3 detectors due to the kinematics of the reaction. Figure 1 shows the energy deposition against ring number in the downstream S3 detector for the contaminated running mode. The kinematic lines of ^{32}Si and ^{196}Pt are clearly separated. As previously discussed, in this mode the beam contained $\approx$10% contamination from ^{96}Mo. Target scatters originating from this contamination can be seen crossing the ^{32}Si kinematic line at higher ring numbers. This contamination will contribute to the excitation of ^{196}Pt target nuclei and therefore to the ^{196}Pt γ-ray intensities. The contamination was accounted for, when extracting γ-ray intensities, due to the dramatically different kinematics for ^{196}Pt target scatters from ^{96}Mo projectiles when compared to ^{32}Si projectile scatters off ^{196}Pt target ions, yielding a resolvable difference in the Doppler reconstruction. Figure 2 shows γ-ray spectra Doppler corrected for the ^{32}Si kinematic solution with the detection of the ^{32}Si downstream, ^{196}Pt downstream and ^{32}Si upstream. In both cases of the downstream detection a significant background is seen at high γ-ray energy, likely due to compound nuclear reactions on low-Z contaminants in the target (i.e., carbon and oxygen). This does not impact the following Coulomb-excitation analysis.

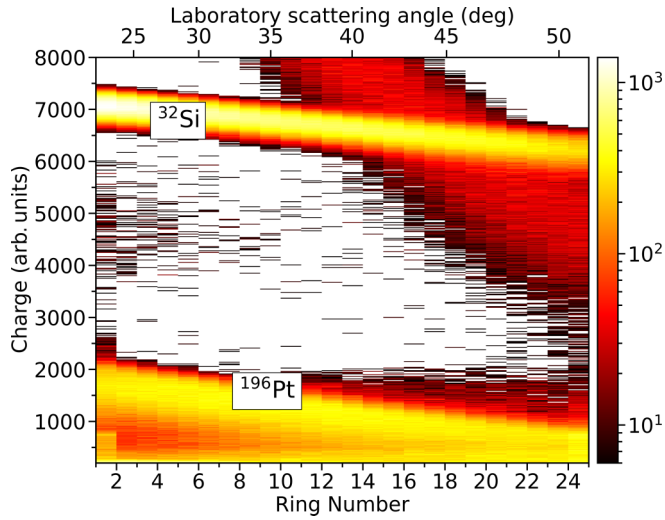

FIG. 1. Charge collected in the JANUS downstream S3 detector against ring number. Corresponding laboratory scattering angles are shown on the top axis. The data shown were acquired at a beam energy of 3.57 MeV/u. The kinematic lines corresponding to the scatter of ^{32}Si and ^{196}Pt nuclei are labeled. The kinematic line corresponding to target scatters from ^{96}Mo, a contaminant in the beam, can also be seen. Note that bins with five or fewer counts are excluded from this figure to aid clarity.

Coulomb-excitation yields were evaluated using the GOSIA code [25] and a χ^2 minimization was performed using the MIGRAD algorithm in the MINUIT library [26] in the ROOT framework to determine transition matrix elements [27]. The data were divided into the following center-of-mass angles: for beam scattered particles detected in both downstream and upstream detectors, 25°–40°, 40°–51°, 51°–60°, 140°–147°, and 147°–164°; for target scattered particles detected in the downstream detector only, 95°–113° and 113°–136°. A simultaneous fitting of ^{196}Pt $2_1^+ \rightarrow 0_1^+$ and $4_1^+ \rightarrow 2_1^+$ γ-ray intensities was used to provide a target normalization, accounting for systematic uncertainties arising in the experimental setup and therefore allowing for the calculation of

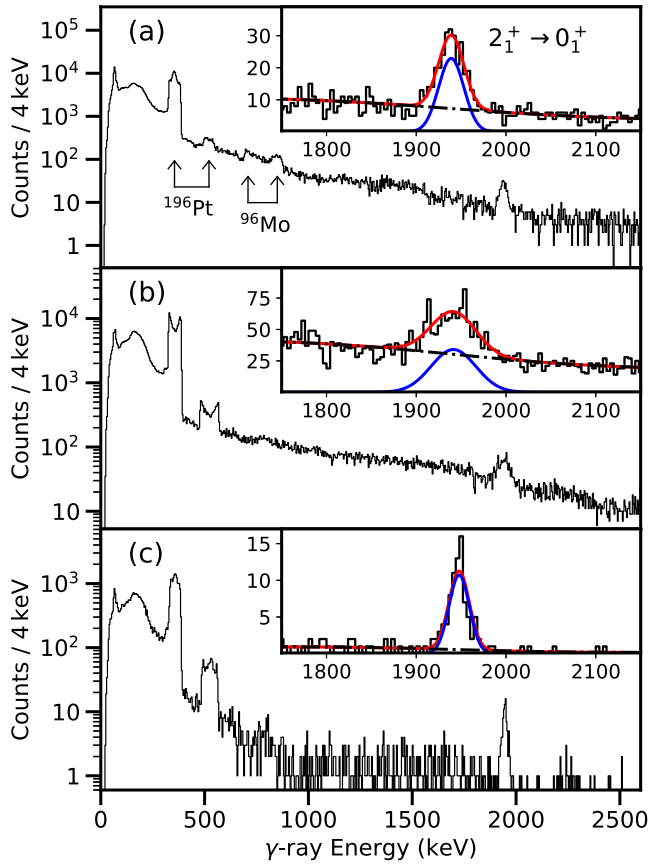

FIG. 2. Doppler-corrected energy spectrum of ^{32}Si γ rays detected in coincidence with a scattered particle of (a) ^{32}Si detected in the downstream S3 detector, (b) ^{196}Pt detected in the downstream S3 detector, or (c) ^{32}Si detected in the upstream S3 detector. The data shown were acquired at a beam energy of 3.57 MeV/u (contaminated). The $2_1^+ \rightarrow 0_1^+$ transition in ^{32}Si is labeled in (a). The insets show the same corresponding spectrum, expanded around the $2_1^+ \rightarrow 0_1^+$ transition peak, with the Gaussian plus background fits applied. Peaks corresponding to transitions in ^{196}Pt and ^{96}Mo are labeled in (a). Note the spectrum in panel (c) corresponds to center-of-mass angles where the minimum impact parameter did not satisfy the Cline criterion and therefore were excluded in the analysis.

absolute matrix elements in ^{32}Si. Matrix elements of ^{196}Pt were also permitted to vary and contributed to the χ^2 in the minimization routine according to their literature values and uncertainties. The ^{196}Pt matrix elements used in the minimization are given in Table I. Stopping powers used in the GOSIA inputs were taken from SRIM-2010 [28]. The effect of changing the stopping powers on the extracted matrix elements was investigated at the $\pm 10\%$ limit and found to be negligible compared to the statistical uncertainties. In the present framework the contaminated and uncontaminated data were analyzed simultaneously. Figure 3 shows the 1σ χ^2 surface distribution for ^{32}Si.

III. DISCUSSION

The extracted $E2$ matrix elements, $B(E2; 0_1^+ \rightarrow 2_1^+)$ values, and $Q_s(2_1^+)$ values are shown in Table II. The present

TABLE I. Matrix elements for ^{196}Pt used to constrain the present analysis.

J_i^π	J_f^π	$\langle J_i^\pi \vert E2 \vert J_f^\pi \rangle$ (eb)	Ref.
0_1^+	2_1^+	1.172(5)	[17]
2_1^+	2_1^+	0.82(10)	[24]
2_1^+	2_2^+	1.36(1)	[24]
2_1^+	4_1^+	1.91(2)	[24]
2_1^+	0_2^+	0.167(15)	[24]
2_2^+	2_2^+	−0.52(20)	[24]
2_2^+	0_2^+	−0.35(70)	[24]
4_1^+	4_1^+	1.36(16)	[24]
J_i^π	J_f^π	$\langle J_i^\pi \vert M2 \vert J_f^\pi \rangle$ (μ_N)	Ref.
2_1^+	2_2^+	0.0723(64)	[17]

$B(E2; 0_1^+ \rightarrow 2_1^+)$ value agrees with those of Refs. [12,14] but with improved uncertainty, while being inconsistent in excess of 3.5σ with the $B(E2; 0_1^+ \rightarrow 2_1^+)$ value deduced in Ref. [13]. The extracted $Q_s(2_1^+)$ value is found to be positive and inconsistent with zero, indicative of a predominantly oblate configuration. We note here that the agreement of our present result with that of Ref. [14] gives confidence to the $B(E2; 0_1^+ \rightarrow 2_1^+)$ value that was extracted in the same work for ^{34}Si.

In Ref. [29] the authors used two different methods, which both rely on the ^{32}Si $B(E2; 0_1^+ \rightarrow 2_1^+)$ value, to calculate the ratio of the neutron and proton multipole matrix elements, M_n/M_p, for ^{32}Si. This ratio provides useful insight into the relative contributions of protons and neutrons to the collective behavior of the nucleus. Here, for completeness, we reevaluate M_n/M_p using the updated value for $B(E2; 0_1^+ \rightarrow 2_1^+)$ obtained in this work. In the first method, the M_p value is calculated using the ^{32}Si $B(E2; 0_1^+ \rightarrow 2_1^+)$ value from Ref. [14], and the corresponding value in the mirror nucleus, ^{32}Ar, is used to

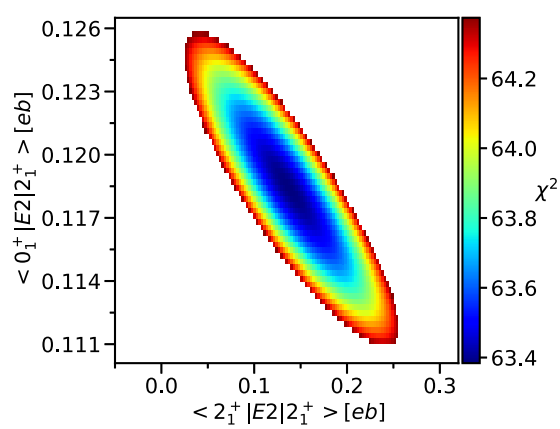

FIG. 3. χ^2 surface plot in ^{32}Si, determined through a comparison of Coulomb-excitation yields and experimental yields using GOSIA [25]. The surface is cut at the $\chi^2 + 1$ limit, demonstrating the preference for a positive $\langle 2_1^+ | E2 | 2_1^+ \rangle$ matrix element. The number of degrees of freedom in the fit was 58, including both experimental data and literature constraints on ^{196}Pt matrix elements.

TABLE II. Reduced matrix elements, reduced transition strengths and spectroscopic quadrupole moments measured in the present work. Literature values are also presented.

$J_i^\pi \to J_f^\pi$	$\langle J_i^\pi \| E2 \| J_f^\pi \rangle$ (eb)	$B(E2)$ (e^2fm^4)	Note
$0_1^+ \to 2_1^+$	0.120(8)	143(20)	This work
		160(60)	[12]
		308(45)	[13]
		113(33)	[14]
$J_i^\pi \to J_i^\pi$	$\langle J_i^\pi \| E2 \| J_i^\pi \rangle$ (eb)	$Q_s(J_i^\pi)$ (eb)	Note
$2_1^+ \to 2_1^+$	0.14(13)	0.11(10)	This work

calculate M_n. The $B(E2; 0_1^+ \to 2_1^+)$ value used for ^{32}Ar was measured in Ref. [29]. In the second method, (p, p') scattering data are used to calculate the M_n/M_p ratio using distorted wave theory. A value $M_n/M_p > N/Z$ is expected in nuclei with a closed proton shell, where the valence neutrons dominate the collective motion. Using the ^{32}Si $B(E2; 0_1^+ \to 2_1^+)$ value from this work, we obtain $M_n/M_p = 1.36(20)$ using the first method, and $M_n/M_p = 1.41^{+0.36}_{-0.20}$ using the second method. Both numbers are consistent with the hydrodynamic result, $N/Z = 1.29$, which assumes neutrons and protons move in phase with the same amplitude, implying that charge and matter distributions are similar [30]. This conclusion on the matter and charge distributions will be used later in the text in our discussion of the axial nature of ^{32}Si.

Figures 4(a) and 4(b) show $B(E2; 0_1^+ \to 2_1^+)$ values for silicon isotopes and $N = 18$ isotones, respectively. Values are compared to shell-model calculations performed in KSHELL [33] using the USDB interaction [11], with effective charges of $e_\pi = 1.35$ and $e_\nu = 0.35$, with a harmonic oscillator form $\hbar\omega = 45A^{-1/3} - 25A^{-2/3}$. Also shown are *ab initio* valence-space in-medium similarity-renormalization-group (VS-IMSRG) calculations [34] performed using two different NN + 3N interactions derived from chiral effective field theory (χEFT), namely 1.8/2.0(EM) [31] and ΔNNLO$_{\rm GO}$(394) [32]. Calculations were also performed using the NN + 3N(lnl) [35] interaction but yielded results similar to 1.8/2.0(EM) and are therefore not shown. In the VS-IMSRG, nucleus-by-nucleus valence-space interactions are derived from χEFT through a series of unitary transformations [36] with electromagnetic operators evolved consistently [37]. While in principle this should provide a near-exact result, a truncation to the evolution of the electromagnetic operators at the two-body level [the IMSRG(2) approximation] is required in order to make the problem computationally tractable due to induced many-body interactions. It has been shown [38,39] that this results in an underprediction of $E2$ matrix elements by 25%. It is seen that, as expected, the USDB $B(E2; 0_1^+ \to 2_1^+)$ calculations reproduce the lighter silicon isotopes, ^{28,30}Si, well, with good reproduction of the $N = 18$ isotones as well. Both of the VS-IMSRG calculations consistently underpredict the $B(E2; 0_1^+ \to 2_1^+)$ values in the lighter silicon isotopes and $N = 18$ isotones; however, when the deficiencies in the computation discussed above are taken

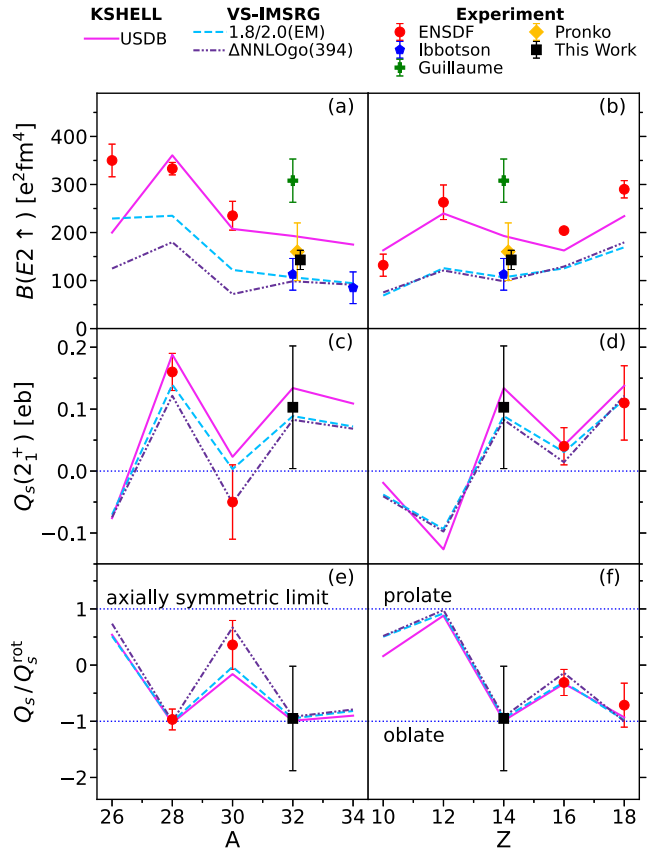

FIG. 4. $B(E2; 0_1^+ \to 2_1^+)$ [$B(E2\uparrow)$], $Q_s(2_1^+)$, and $Q_s(2_1^+)/Q_s(2_1^+)^{\rm rot}$ ($Q_s/Q_s^{\rm rot}$) values [(a), (c), and (e)] for the silicon isotopes $26 \leqslant A \leqslant 34$, and [(b), (d), and (f)] $N = 18$ isotones between $10 \leqslant Z \leqslant 18$. The results of the current work are shown as black squares. The $Q_s(2_1^+)/Q_s(2_1^+)^{\rm rot}$ values are calculated using Eq. (5). The horizontal dotted lines in (c), (d), (e), and (f) are shown to guide the eye. In (c) and (d) the single dotted line corresponds to $Q_s(2_1^+) = 0$ (e.g., a spherical shape), while in (e) and (f) the pair of dotted lines correspond to $Q_s(2_1^+)/Q_s(2_1^+)^{\rm rot}$ values for prolate and oblate shapes in the axially symmetric limit, as indicated. Theoretical calculations from shell model (USDB) and *ab initio* (VS-IMSRG) approaches are also shown. Two different interactions derived from χEFT are used for the VS-IMSRG calculations (1.8/2.0(EM) [31], ΔNNLO$_{\rm GO}$(394) [32]).

into account, there is good agreement with the experimental data, especially for the 1.8/2.0(EM) interaction.

At this point it is worth highlighting the differences in low-lying structure between ^{32}Si and ^{34}Si. At $N = 18$, ^{32}Si has been shown to be a pure *sd*-shell nucleus at low excitation energy, with no *pf* excitations required to reproduce low-lying excited states [12,14,40], similar to ^{28}Ne and ^{30}Mg [41,42]. ^{34}Si, by comparison, is predominantly *sd* in its ground state, but the first (0_2^+) and second (2_1^+) excited states are dominated by intruder configurations from *pf* excitations. It is therefore expected that the $B(E2; 0_1^+ \to 2_1^+)$ value calculated in the *sd* shell fails to reproduce the experimental value for ^{34}Si. Indeed, in Ref. [43], it was shown that by using the *sdpfu*-mix interaction [44] the $B(E2; 2_1^+ \to 0_1^+)$ in ^{34}Si could be well reproduced. ^{32}Si therefore stands out as an outlier in

$B(E2;0_1^+ \to 2_1^+)$ values when compared to appropriate shell-model calculations.

Although the $B(E2;0_1^+ \to 2_1^+)$ value is considerably lower than anticipated from theoretical calculations, when computational deficiencies in the VS-IMSRG calculations are taken into account, Figs. 4(c) and 4(d) show rather good agreement with theory for $Q_s(2_1^+)$ in the silicon isotopes and $N = 18$ isotones, respectively. Indeed, while the $Q_s(2_1^+)$ values are associated with larger uncertainties than their respective $B(E2;0_1^+ \to 2_1^+)$ values, the agreement with theoretical predictions is typically excellent for all cases where data exists. In an effort to understand this apparent contradiction, we compare the obtained static quadrupole moment to the predicted value for an axially symmetric rotor in the Bohr-Mottelson model [45]. In this model the $B(E2)$ values and static quadrupole moments are defined by a single parameter, the intrinsic quadrupole moment, Q_0:

$$B(E2;I_i \to I_f)^{\text{rot}} = \frac{5}{16\pi} Q_0^2 |\langle I_i K 20 | I_f K\rangle|^2, \tag{1}$$

$$Q_s(I)^{\text{rot}} = \frac{3K^2 - I(I+1)}{(I+1)(2I+3)} Q_0, \tag{2}$$

where K is the projection of the total angular momentum of the state on to the symmetry axis. For the case $K = 0$ (ground-state rotational band of an even-even nucleus), $I_i = 0$ and $I_f = 2$, Eqs. (1) and (2) simplify to

$$B(E2;0 \to 2)^{\text{rot}} = \frac{5}{16\pi} Q_0^2, \tag{3}$$

$$Q_s(2)^{\text{rot}} = -\frac{2}{7} Q_0. \tag{4}$$

The reduced quadrupole moment is defined as the ratio of the experimentally measured static quadrupole moment to the value predicted by the rotational model:

$$\frac{Q_s(2_1^+)}{Q_s(2_1^+)^{\text{rot}}} = -\frac{7}{2}\sqrt{\frac{5}{16\pi}} \frac{Q_s(2_1^+)}{\sqrt{B(E2\uparrow)}}, \tag{5}$$

which gives a quantitative description of how well the axially symmetric rotational model approximates the true nature of the nucleus [46]. For an axial shape the $Q_s(2_1^+)/Q_s(2_1^+)^{\text{rot}}$ value becomes $+1$ in the prolate case and -1 in the oblate case. Values between 1 and -1 are an indication of triaxiality. Experimental and theoretical values for $Q_s(2_1^+)/Q_s(2_1^+)^{\text{rot}}$ are plotted in Figs. 4(e) and 4(f) for Si isotopes and $N = 18$ isotones, respectively. The central value for $Q_s(2_1^+)/Q_s(2_1^+)^{\text{rot}}$ obtained for ^{32}Si is $-0.95(93)$, within 1σ of the rigid oblate limit and both the USDB and VS-IMSRG calculations, though with a large uncertainty.

The only rigorous approach to relate the parameters describing the intrinsic shape of the charge distribution to laboratory-frame observables is using the method developed by Kumar and Cline [20,47], which constructs rotationally invariant zero-coupled products from the electric multipole transition operator through the use of sum rules. Under the assumption that the charge and matter distributions are equivalent, which is supported by the consistent agreement between M_n/M_p and the hydrodynamic result N/Z, and, through a reduced sum containing only the first-excited 2^+ state, one obtains the approximation

$$\cos(3\gamma) \approx \frac{Q_s(2_1^+)}{Q_s(2_1^+)^{\text{rot}}} \tag{6}$$

for the ground state of an even-even nucleus [48]. This approximation should be treated with caution since it is well known that higher-lying 2^+ states can have a significant contribution to the quadrupole strength. In the case of ^{32}Si, the lifetime of the 2_2^+ state has been measured to be 0.26(9) ps, and the branching and mixing ratios to the 2_1^+ state are known [12]. Although the $Q_s(2_2^+)$ value is unknown, its contribution to $\cos(3\gamma)$ is expected to be negligible compared to the contribution from $B(E2;2_1^+ \to 2_2^+)$ [49]. Using the available experimental data, the contribution to $\cos(3\gamma)$ of the 2_2^+ state is around 5%, similar to that predicted by the USDB interaction, and negligible compared to the uncertainty on $Q_s(2_1^+)$. It has been shown in Ref. [48] that the approximate determination of $\cos(3\gamma)$ in Eq. (6) deviates from the true value by $0.26^{+0.42}_{-0.37}$, though for many of the nuclei included in this study the 2_2^+ has a large contribution to the final $\cos(3\gamma)$ value. Therefore, for ^{32}Si, an approximate value for $\cos(3\gamma)$ can be obtained using Eq. (6). Note that, due to the intruder nature of the 2_1^+ state in ^{34}Si, the assumption made in Eq. (6) is not valid for this nucleus.

The approximation in Eq. (6) is to exclude contributions to the invariant sum from products of $E2$ matrix elements beyond the 2_1^+ state. By using the method outlined in Ref. [50], invariants can be calculated within the shell model that are exact within the model space and do not rely on a potentially incomplete summation. As shown in Fig. 5, the effect of this exact solution is to introduce a triaxial component to the central deformation, as well as softness in both the β and γ parameters. If the overprediction of $B(E2;0_1^+ \to 2_1^+)$ in the present work is representative of all electric quadrupole strengths, the value shown in Fig. 5 would correspond to an overprediction in the central value of β of approximately 15%.

While the uncertainties associated with $\cos(3\gamma)$ are significant, we find that all experimentally available data are well reproduced by both the VS-IMSRG and shell model calculations. This leads to the intriguing conclusion that the models are overpredicting the *scale* of the quadrupole deformation in ^{32}Si, while seeming to reproduce its form. We note that relativistic beyond-mean-field calculations [51] similarly over predict the $B(E2;0_1^+ \to 2_1^+)$ values and, furthermore, are unable to reproduce $Q_s(2_1^+)$.

To investigate the origins of this over prediction of $E2$ strength, a number of shell-model calculations were performed. As expected, ^{32}Si is found in calculations to be a nearly pure sd-shell nucleus in its ground state, with no significant impact from including pf excitations. It was found that the observed $E2$ strength could be reproduced through adjustments to the proton $d_{5/2}$ orbital. As a simple means of testing the relative importance of different single-particle orbits in contributing to the collective nature of the nucleus, one can adjust the effective single-particle energies (ESPEs). Two adjustments to the ESPEs were found to appropriately reduce the calculated $E2$ strength: first, increasing the binding

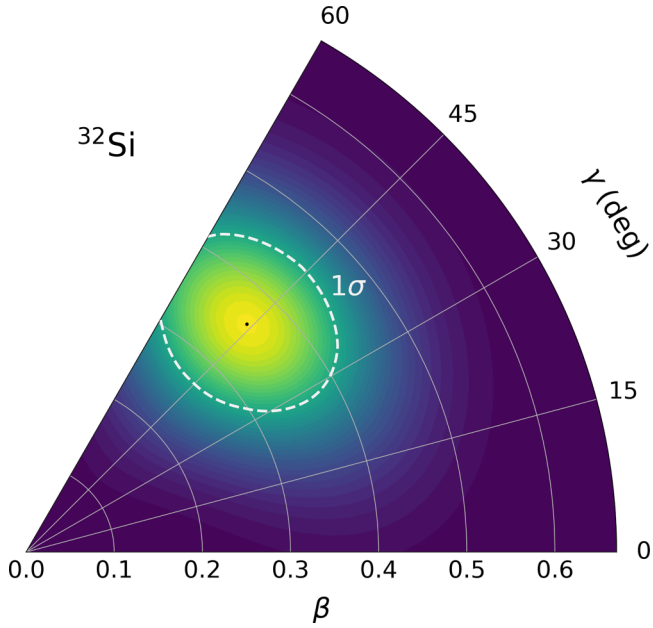

FIG. 5. β-γ plot for ^{32}Si from USDB shell-model calculations. The central values are $\beta = 0.36$ and $\gamma = 46^\circ$, with fluctuations $\sigma(\beta) = 0.09$ and $\sigma(\gamma) = ^{+14^\circ}_{-18^\circ}$. These are calculated using quadrupole invariants [20,47] and are exact within the model space. The 1σ limit, corresponding to the softness of the nuclear shape, is shown as a dashed white line. The fluctuations in β and γ show a softness similar to calculations for other nuclei in this region [50].

of the $\pi d_{5/2}$ orbital by approximately 1 MeV, and second, increasing the spin-orbit splitting of the proton $d_{5/2}$-$d_{3/2}$ orbitals by approximately 1 MeV. A splitting of this kind can be achieved in the heavier silicon isotopes since the additional neutrons will occupy single-particle levels which will increase the proton $d_{5/2}$-$d_{3/2}$ splitting through the tensor force [52]. In both cases the $E2$ strength was reduced to the level of the experimental values, while the $Q_s(2_1^+)$ values remained largely unchanged. The occupancy of the $\pi d_{5/2}$ orbital is in fact particularly critical, since blocking it altogether reduces the $B(E2; 0_1^+ \to 2_1^+)$ value by a factor of 15. While modifying the ESPEs is an appealing fix, care has to be taken since a larger systematic study, including excitations to the pf space, would be required to fully appreciate the effect of changing ESPEs in this region, which is beyond the scope of the present study, and we stress that this is no more than a simple exercise to demonstrate the role of different single-particle orbits.

With this in mind, when moving to ^{34}Si, the ground state is nearly pure sd, but the first and second excited states are both pf intruders. Without modification, the $sdpfu$-mix interaction reproduces $B(E2; 0_1^+ \to 2_1^+)$ values for the $N = 20$ isotones. Of some interest then is how the adjustments to the ESPEs, required to reproduce the ^{32}Si $E2$ strengths, impact ^{34}Si and other $N = 20$ nuclides. It was found that, with the second proposed solution (broadening the $d_{5/2}$-$d_{3/2}$ splitting), the nuclei at $N = 20$ remain well reproduced by the $sdpfu$-mix interaction. The first solution (increasing the $d_{5/2}$ binding), however, resulted in the intruder 0_2^+ state in ^{34}Si having too high excitation energy. $B(E2)$ transition strengths were then compared to those for the second 2^+ state in ^{32}Si, for which experimental data are available [12]. Here, it was found that increasing the $d_{5/2}$-$d_{3/2}$ splitting caused the ratio of $B(E2; 2_1^+ \to 0_1^+)/B(E2; 2_2^+ \to 0_1^+)$ to deviate significantly from experimental values, a ratio that was well reproduced with unadjusted calculations. Based on the above investigation, there was no adjustment to the ESPEs that could simultaneously reproduce $E2$ observables in both ^{32}Si and ^{34}Si.

With the above discussion in mind, the disagreement in the VS-IMSRG calculations is intriguing, with ^{26,28,30}Si all well reproduced when the empirical correction of Ref. [39] is incorporated. In that work, a comparison with configuration interaction calculations was used to demonstrate the importance of multiparticle multihole (mp-mh) excitations which were necessarily lost in the operator evolution due to the IMSRG(2) approximation. Here, we find that the experimental data lie between the corrected and uncorrected VS-IMSRG values, which presents the possibility that these mp-mh contributions are somehow suppressed in ^{32}Si. The reader will note that these mp-mh contributions, suppressed in the IMSRG(2) approximation, bear some similarity to the core-polarization effects that shell-model effective charges account for. Furthermore, the overprediction of $E2$ strength in the VS-IMSRG method cannot easily be explained through changes in the $d_{5/2}$ energy. Through the interaction evolution, the method is perhaps uniquely sensitive to nucleus-by-nucleus changes to orbitals and would therefore be expected to capture any such effects. We therefore propose a single explanation which reconciles the deficiencies in both models: that there is a reduction in out-of-space, core-polarization contributions to the $E2$ strength in ^{32}Si.

IV. CONCLUSIONS

In conclusion, we present a low-energy Coulomb excitation measurement of ^{32}Si. From the first determination of $Q_s(2_1^+)$ and an improved measurement of $B(E2; 0_1^+ \to 2_1^+)$ we are able to demonstrate the weakly deformed, centrally oblate nature of the nucleus. While phenomenological and *ab initio* calculations are able to reproduce the oblate structure, they consistently overpredict the absolute scale of deformation. Through comparison with shell-model calculations we demonstrate the essential role of the $\pi d_{5/2}$ orbital, with adjustments to its binding, and the proton $d_{5/2}$-$d_{3/2}$ spin-orbit splitting, allowing for the reproduction of the experimental data. Expanding the comparison to ^{34}Si and incorporating pf excitations, we find that, of the two modifications to the ESPEs, the solution involving an enhanced $d_{5/2}$-$d_{3/2}$ splitting offers the best reproduction of the available data. However, this solution fails to reproduce the quadrupole strength of the 2_2^+ state in ^{32}Si. Intriguingly, we find that a comparison with *ab initio* valence-space in-medium similarity renormalizartion group calculations also fails to reproduce ^{32}Si, when an empirical correction for missing $E2$ strength is included. That the VS-IMSRG calculations better reproduce the experimental values without the inclusion of the empirical correction might be indicative of a reduced contribution from multiparticle, multihole excitations in this nucleus.

ACKNOWLEDGMENTS

The authors thank the beam-delivery team at the National Superconducting Cyclotron Laboratory for providing a high-quality beam. Work at the University of Surrey was supported under UKRI Future Leaders Fellowship Grant No. MR/T022264/1 and by the Science and Technologies Facilities Council (STFC). The work was supported by U.S. DOE Contract No. 89233218CNA000001, by the U.S. Department of Energy, Office of Science, Office of Nuclear Physics, under Contract No. DE-AC02-06CH11357 (ANL) and under Grant No. DE-SC0020451 (MSU), by the U.S. National Science Foundation (NSF) under Grant No. PHY-1565546, by the DOE National Nuclear Security Administration through the Nuclear Science and Security Consortium under Award No. DE-NA0003180, by NSERC under Grants No. SAPIN-2018-00027 and No. RGPAS-2018-522453, and by the Arthur B. McDonald Canadian Astroparticle Physics Research Institute. Work at Lawrence Livermore National Laboratory was performed under the auspices of the U.S. Department of Energy under Contract No. DE-AC52-07NA27344. A.P. is supported by Grants No. CEX2020-001007-S funded by MCIN/AEI/10.13039/501100011033 and No. PID2021-127890NB-I00. Computations were performed with an allocation of computing resources on Cedar at WestGrid and Compute Canada.

[1] T. Motobayashi, Y. Ikeda, K. Ieki, M. Inoue, N. Iwasa, T. Kikuchi, M. Kurokawa, S. Moriya, S. Ogawa, H. Murakami, S. Shimoura, Y. Yanagisawa, T. Nakamura, Y. Watanabe, M. Ishihara, T. Teranishi, H. Okuno, and R. Casten, Phys. Lett. B **346**, 9 (1995).

[2] C. E. Svensson, A. O. Macchiavelli, A. Juodagalvis, A. Poves, I. Ragnarsson, S. Åberg, D. E. Appelbe, R. A. E. Austin, C. Baktash, G. C. Ball, M. P. Carpenter, E. Caurier, R. M. Clark, M. Cromaz, M. A. Deleplanque, R. M. Diamond, P. Fallon, M. Furlotti, A. Galindo-Uribarri, R. V. F. Janssens *et al.*, Phys. Rev. Lett. **85**, 2693 (2000).

[3] J. Dowie, T. Kibédi, D. Jenkins, A. Stuchbery, A. Akber, H. Alshammari, N. Aoi, A. Avaa, L. Bignell, M. Chisapi, B. Coombes, T. Eriksen, M. Gerathy, T. Gray, T. Hoang, E. Ideguchi, P. Jones, M. Kumar Raju, G. Lane, B. McCormick *et al.*, Phys. Lett. B **811**, 135855 (2020).

[4] F. M. Prados Estévez, A. M. Bruce, M. J. Taylor, H. Amro, C. W. Beausang, R. F. Casten, J. J. Ressler, C. J. Barton, C. Chandler, and G. Hammond, Phys. Rev. C **75**, 014309 (2007).

[5] K. Hadyńska-Klęk, P. J. Napiorkowski, M. Zielińska, J. Srebrny, A. Maj, F. Azaiez, J. J. Valiente Dobón, M. Kicińska Habior, F. Nowacki, H. Naïdja, B. Bounthong, T. R. Rodríguez, G. de Angelis, T. Abraham, G. Anil Kumar, D. Bazzacco, M. Bellato, D. Bortolato, P. Bednarczyk, G. Benzoni *et al.*, Phys. Rev. Lett. **117**, 062501 (2016).

[6] K. Wimmer, T. Kröll, R. Krücken, V. Bildstein, R. Gernhäuser, B. Bastin, N. Bree, J. Diriken, P. Van Duppen, M. Huyse, N. Patronis, P. Vermaelen, D. Voulot, J. Van de Walle, F. Wenander, L. M. Fraile, R. Chapman, B. Hadinia, R. Orlandi, J. F. Smith *et al.*, Phys. Rev. Lett. **105**, 252501 (2010).

[7] T. Baumann, A. M. Amthor, D. Bazin, B. A. Brown, C. M. F. III, A. Gade, T. N. Ginter, M. Hausmann, M. Matoš, D. J. Morrissey, M. Portillo, A. Schiller, B. M. Sherrill, A. Stolz, O. B. Tarasov, and M. Thoennessen, Nature (London) **449**, 1022 (2007).

[8] E. Caurier, G. Martínez-Pinedo, F. Nowacki, A. Poves, and A. P. Zuker, Rev. Mod. Phys. **77**, 427 (2005).

[9] N. Tsunoda, T. Otsuka, K. Takayanagi, N. Shimizu, T. Suzuki, Y. Utsuno, S. Yoshida, and H. Ueno, Nature (London) **587**, 66 (2020).

[10] G. R. Jansen, J. Engel, G. Hagen, P. Navrátil, and A. Signoracci, Phys. Rev. Lett. **113**, 142502 (2014).

[11] B. A. Brown and W. A. Richter, Phys. Rev. C **74**, 034315 (2006).

[12] J. G. Pronko and R. E. McDonald, Phys. Rev. C **6**, 2065 (1972).

[13] G. Guillaume, B. Rastegar, P. Fintz, and A. Gallmann, Nucl. Phys. A **227**, 284 (1974).

[14] R. W. Ibbotson, T. Glasmacher, B. A. Brown, L. Chen, M. J. Chromik, P. D. Cottle, M. Fauerbach, K. W. Kemper, D. J. Morrissey, H. Scheit, and M. Thoennessen, Phys. Rev. Lett. **80**, 2081 (1998).

[15] A. Villari, D. Alt, G. Bollen, D. Crisp, M. Ikegami, S. Krause, A. Lapierre, S. Lidia, D. Morrissey, S. Nash *et al.*, *Proceedings of the 7th International Particle Accelerator Conference, IPAC2016, May 8–13, Busan, Korea* (JACoW, Geneva, 2016), p. 1287.

[16] A. Gade and B. M. Sherrill, Phys. Scr. **91**, 053003 (2016).

[17] From ENSDF database as of January 11th 2024. Version available at http://www.nndc.bnl.gov/ensarchivals/.

[18] E. Lunderberg, J. Belarge, P. Bender, B. Bucher, D. Cline, B. Elman, A. Gade, S. Liddick, B. Longfellow, C. Prokop, D. Weisshaar, and C. Wu, Nucl. Instrum. Methods Phys. Res., Sect. A **885**, 30 (2018).

[19] Micron Semiconductor Ltd., Micron catalogue, 2019.

[20] D. Cline, Annu. Rev. Nucl. Part. Sci. **36**, 683 (1986).

[21] W. Mueller, J. Church, T. Glasmacher, D. Gutknecht, G. Hackman, P. Hansen, Z. Hu, K. Miller, and P. Quirin, Nucl. Instrum. Methods Phys. Res., Sect. A **466**, 492 (2001).

[22] P. Bender, https://github.com/pcbend/GRUTinizer/, 2022.

[23] R. Brun and F. Rademakers, Nucl. Instrum. Methods Phys. Res., Sect. A **389**, 81 (1997).

[24] C. Lim, R. Spear, M. Fewell, and G. Gyapong, Nucl. Phys. A **548**, 308 (1992).

[25] T. Czosnyka, D. Cline, and C. Y. Wu, Bull. Am. Phys. Soc **28**, 745 (1983).

[26] F. James and M. Roos, Comput. Phys. Commun. **10**, 343 (1975).

[27] J. Henderson, https://github.com/jhenderson88/GOSIAFitter.

[28] J. F. Ziegler, M. Ziegler, and J. Biersack, 19th International Conference on Ion Beam Analysis, Nucl. Instrum. Methods Phys. Res. Sect. B **268**, 1818 (2010).

[29] P. D. Cottle, Z. Hu, B. V. Pritychenko, J. A. Church, M. Fauerbach, T. Glasmacher, R. W. Ibbotson, K. W. Kemper, L. A. Riley, H. Scheit, and M. Steiner, Phys. Rev. Lett. **88**, 172502 (2002).

[30] A. Bernstein, V. Brown, and V. Madsen, Phys. Lett. B **103**, 255 (1981).

[31] K. Hebeler, S. K. Bogner, R. J. Furnstahl, A. Nogga, and A. Schwenk, Phys. Rev. C **83**, 031301(R) (2011).

[32] W. G. Jiang, A. Ekström, C. Forssén, G. Hagen, G. R. Jansen, and T. Papenbrock, Phys. Rev. C **102**, 054301 (2020).
[33] N. Shimizu, T. Mizusaki, Y. Utsuno, and Y. Tsunoda, Comput. Phys. Commun. **244**, 372 (2019).
[34] S. R. Stroberg, S. K. Bogner, H. Hergert, and J. D. Holt, Annu. Rev. Nucl. Part. Sci. **69**, 307 (2019).
[35] V. Somà, P. Navrátil, F. Raimondi, C. Barbieri, and T. Duguet, Phys. Rev. C **101**, 014318 (2020).
[36] S. R. Stroberg, A. Calci, H. Hergert, J. D. Holt, S. K. Bogner, R. Roth, and A. Schwenk, Phys. Rev. Lett. **118**, 032502 (2017).
[37] N. M. Parzuchowski, S. R. Stroberg, P. Navrátil, H. Hergert, and S. K. Bogner, Phys. Rev. C **96**, 034324 (2017).
[38] J. Henderson *et al.*, Phys. Lett. B **782**, 468 (2018).
[39] S. R. Stroberg, J. Henderson, G. Hackman, P. Ruotsalainen, G. Hagen, and J. D. Holt, Phys. Rev. C **105**, 034333 (2022).
[40] H. T. Fortune, L. Bland, D. L. Watson, and M. A. Abouzeid, Phys. Rev. C **25**, 5 (1982).
[41] O. Niedermaier, H. Scheit, V. Bildstein, H. Boie, J. Fitting, R. von Hahn, F. Köck, M. Lauer, U. Pal, H. Podlech, R. Repnow, D. Schwalm, C. Alvarez, F. Ames, G. Bollen, S. Emhofer, D. Habs, O. Kester, R. Lutter, K. Rudolph *et al.*, Proceedings of the 22nd International Nuclear Physics Conference, Part 2, Nucl. Phys. A **752**, 273 (2005).
[42] H. Iwasaki, T. Motobayashi, H. Sakurai, K. Yoneda, T. Gomi, N. Aoi, N. Fukuda, Z. Fülöp, U. Futakami, Z. Gacsi, Y. Higurashi, N. Imai, N. Iwasa, T. Kubo, M. Kunibu, M. Kurokawa, Z. Liu, T. Minemura, A. Saito, M. Serata *et al.*, Phys. Lett. B **620**, 118 (2005).
[43] F. Rotaru, F. Negoita, S. Grévy, J. Mrazek, S. Lukyanov, F. Nowacki, A. Poves, O. Sorlin, C. Borcea, R. Borcea, A. Buta, L. Cáceres, S. Calinescu, R. Chevrier, Z. Dombrádi, J. M. Daugas, D. Lebhertz, Y. Penionzhkevich, C. Petrone, D. Sohler *et al.*, Phys. Rev. Lett. **109**, 092503 (2012).
[44] E. Caurier, F. Nowacki, and A. Poves, Phys. Rev. C **90**, 014302 (2014).
[45] A. Bohr and B. Mottelson, *Nuclear Structure, Volume II: Nuclear Deformations* (W. A. Benjamin, New York, 1975).
[46] S. J. Q. Robinson, A. Escuderos, L. Zamick, P. von Neumann-Cosel, A. Richter, and R. W. Fearick, Phys. Rev. C **73**, 037306 (2006).
[47] K. Kumar, Phys. Rev. Lett. **28**, 249 (1972).
[48] J. Henderson, Phys. Rev. C **102**, 054306 (2020).
[49] W. Andrejtscheff and P. Petkov, Phys. Lett. B **329**, 1 (1994).
[50] A. Poves, F. Nowacki, and Y. Alhassid, Phys. Rev. C **101**, 054307 (2020).
[51] X.-Y. Wu and X.-R. Zhou, Phys. Rev. C **92**, 054321 (2015).
[52] T. Otsuka, T. Suzuki, R. Fujimoto, H. Grawe, and Y. Akaishi, Phys. Rev. Lett. **95**, 232502 (2005).